Journal of Non-Crystalline Solids 555 (2021) 120619

Contents lists available at ScienceDirect

Journal of Non-Crystalline Solids

journal homepage: www.elsevier.com/locate/jnoncrysol

Investigation of ZnSe stability and dissolution behavior in As-S-Se chalcogenide glasses

Matthieu Chazot [a,*], Chanelle Arias [a], Myungkoo Kang [a], Cesar Blanco [a], Alexandros Kostogiannes [a], Justin Cook [a], Anupama Yadav [a], Vincent Rodriguez [b], Frederic Adamietz [b], Dominique Verreault [b], Sylvain Danto [c], Thomas Loretz [d], Angela Seddon [e], David Furniss [e], Kenneth Schepler [a], Martin C. Richardson [a], Kathleen A. Richardson [a]

[a] CREOL, College of Optics and Photonics, University of Central Florida, Orlando, FL 32816, USA
[b] Université de Bordeaux, Institut des Sciences Moléculaires, CNRS UMR 5255, 351 cours de la libération, 33405 Talence cedex, France
[c] Université de Bordeaux, ICMCB, CNRS UMR 5026, 87 Avenue du Dr Albert Schweitzer, 33600 Pessac, France
[d] Computer Engineering Service, 5618 Shenandoah Drive, Waxhaw, NC 28173-6860, USA
[e] Mid-Infrared Photonics Group, George Green Institute for Electromagnetics Research, Faculty of Engineering, University of Nottingham, NG7 2RD, UK

A B S T R A C T

Optical composite fibers based on active transition metal (TM)-doped semiconductor crystals are being investigated for use in mid-infrared (mid-IR) fiber laser systems. This study evaluates a candidate glass matrix system assessing its key physical properties and suitability for optical fiber drawing and examines the stability of TM-doped ZnSe crystals during processing. Results indicate that despite excellent refractive index matching between crystal and glass matrix and good fiber draw attributes, the stability of the crystalline dopant within the glass melt is severely impacted by melt conditions. The time and temperature dependence of this stability is mapped by X-ray diffraction (XRD) and second-harmonic generation (SHG) microscopy, illustrating how these tools can be used to track the phase stability and robustness throughout the melting process. Results show that in a range of sulfo-selenide based matrices, dissolution and re-precipitation of Zn-containing crystalline phases is a dominant mechanism.

1. Introduction

Chalcogenide glasses (ChGs) are non-oxide glasses, which transmit in the infrared (IR) portion of the spectrum. They are based typically on Group XIV, XV and XVI elements within the periodic table, excluding oxygen, and owe their excellent IR transmission and tailorable optical and physical properties to their broad glass forming tendency [1]. Recently, efforts have examined how further compositional development of these chalcogenide glasses might be extended to enable their use in more diverse applications, such as mid-infrared (mid-IR) laser sources, where their intrinsic limitations of low glass transition temperature, limited thermal and mechanical stability, and active optical (luminescent) performance can be overcome [2–5]. Mid-IR sources which emit in the 3–5 μm spectral window are of interest for numerous applications including medical imaging and diagnostics, remote sensing of chemicals, and IR countermeasures against heat-seeking missiles [6]. In a recent review, Jackson and Jain [2] reported that production of mid-IR fiber laser sources that emit at wavelengths longer than 4 μm is extremely difficult with currently available mid-IR glass fibers, due largely to difficulties in achieving population inversion at such wavelengths. One unique approach to overcome this issue is through the introduction of a secondary active species in a chalcogenide glass matrix. The use of secondary crystalline species to form such a multiphase optical composite has already shown some success, by enabling tailorable modification of broadband refractive index and dispersion properties in passive chalcogenide-based glass ceramics [7,8]. However, other challenges as summarized here remain. Multiple studies have explored the use of composites as an approach towards creation of optically active material suitable for use as a novel laser medium in the mid-IR [6,9]. The introduction of species such as transition metal (TM)-doped nano/micro-crystals homogeneously dispersed within an optical glass would enable formation of an optical composite whose optical function blends the performances of both glass host and dopant. However, as in all active materials, the environment of the dopant species within the glass matrix as well as its stability during matrix processing and component forming, requires optimization so that emissive performance during use can be maintained. Thus, parallel examination of both new host and dopant materials continue to be

* Corresponding author.
E-mail address: matthieuanthonyalexandre.chazot@ucf.edu (M. Chazot).

https://doi.org/10.1016/j.jnoncrysol.2020.120619
Received 20 November 2020; Received in revised form 17 December 2020; Accepted 18 December 2020

explored for this important spectral window.

Bulk crystalline Fe^{2+}:ZnSe has been shown to demonstrate lasing in the 3-5 μm range due to its crystal field environment that ensures a tetrahedral coordination of the TM ions [10–12]. This dopant/crystal environment results in broad absorption and emission bands due to a strong electron-phonon coupling between the lattice and the active ions [10,13]. A similar local environment cannot be directly achieved in a glass host due to the disordered network environments associated with the glass structure. To enable application diversity, it is also desirable to have such emission in a flexible form factor such as an optical fiber, for implementation in high quality mid-IR fiber lasers that can remain stable against misalignment while possessing physical properties compatible with any cooling required to maintain beam quality control for high power loading. While recent efforts [14] to integrate crystalline media in the core of glass drawn into fiber has been explored, phase stability and loss levels still do not reach those for glass-only media. Such a fiber form factor, is not easily realized with crystalline media, where control of fiber core/cladding compositions and dimensions are challenging and long lengths are impossible. Hence alternative strategies to integrate the desirable attributes of the active crystalline species in a medium compatible with fiber formation (i.e., glass), enabling suitably long (up to ~1 m) lengths, suggests the use of a fiber-based optical composite. This concept has been explored by others examining glasses for use in fibers as laser media in the IR [15–19]. As described in these prior studies, the candidate glass for a potential composite system needs to be thermally and chemically compatible with the dopant crystal (the Fe^{2+} ion in the doped Fe:ZnSe crystal) and possess a low loss matrix host suitable for fiberization. Such an optical composite would integrate suitably high loading levels of dopant while maintaining low optical loss (in both absorption and emission bands), allowing the resulting multi-phase preform to maintain its stability required for fiberization. This compatibility with fiber formation is largely defined by the attributes of the parent glass, the stability of the active media (towards dissolution and/or phase change), and the drawing behavior required for such a fiber laser medium, multiple variables which require parallel optimization. While the idea of creating an optical nanocomposite has been attempted previously [3,5,20–23], it has not been entirely successful due to many difficulties. Key challenges remaining include the creation of an optically-tailored base chalcogenide glass matrix (refractive index matched), where the physical dispersion of crystals is ensured (optimization of viscosity/temperature effects), and where the crystallization stability of the glass matrix and the desired primary dopant phase or undesirable secondary phase(s) during the synthesis steps of the composite material, can be definitively controlled and quantified [4]. The recent results in ref 4 suggest such control may be possible, but precise control of the stability against dissolution of the crystals in the matrix, was not independently and conclusively shown by multiple tools or in experiments aimed at duplicating these results. Thus, to realize the ultimate performance of this composite, it is necessary to separate these multiple variables and to understand the multi-phase chemistry and crystallization kinetics of the system.

The classic way to prepare a ZnSe/ChG composite is using the so-called “grinding remelt” technique. This method involves a two-step process; here, a previously prepared ChG matrix material is ground and mixed with doped crystalline powders, (ZnSe in this case) prior to a remelt process [4,21]. This protocol allows for a reduction in the time and the temperature of synthesis required to prepare a homogenous composite material with good optical properties and avoid possible dissolution of the dopant ZnSe crystals. More recently, a new approach employing the fabrication of chalcogenide glass ceramic through the precipitation of ZnS/ZnSe nano-crystals has been proposed [24–26]. This method illustrated the possibility to obtain Co/Fe:ZnSe nano-crystals in a chalcogenide bulk glass matrix with reduced scattering losses, where emission in the 2.5-5.5μm spectral range was achieved [24]. However, from the authors’ observation, only a minority (31%) of the post-processed Fe^{2+} ions were found to be in the desirable position within the post-processed ZnSe crystals following crystallization enabling optical emission. The remaining dopant species remained dispersed within the glass matrix, an undesirable result. This highlights a challenge as TM in general are considered to be impurities in chalcogenide glasses and optical fibers, as they are often responsible for introducing strong absorption losses in the IR [27]. Hence, this approach, while clever, could be problematic as the performance of the fiber laser gain media could be significantly diminished because emitted photons would be re-absorbed by the glass matrix.

During compilation of this article a recent report from Coco Jr. et. al., presented demonstration of the first operative continuous wave Fe^{2+}:ZnSe Mid-IR fiber laser [28]. Here, the II-VI crystalline materials were prepared by high pressure chemical vapor deposition (HPCVD) [29] that enable the deposition of Fe^{2+}:ZnSe, ZnS and/or ZnS_xSe_{1-x} to build a core-cladding structure within a silica capillary. Despite the very encouraging results, this route suffers certain limitations. Most notably, the fiber’s physical integrity (as well as it’s optical and mechanical homogeneity) may be compromised by the presence of a hole in the middle of the fiber the short length of the fiber (only ~1 cm in length) as well as the low thermal conductivity of the silica outer cladding. Despite these limitations, the initial optical performance is promising, and the intrinsic capabilities of a vapor phase processing approach offers chemical compositional flexibility. Other options are under investigation such as the development of new glass matrix with better thermal properties or the deposition of diamond layer that could interface between the silica cladding and the II-VI crystal core structure [28]. A further report by the group has shown promise in using the same chemical vapor transport as a means towards filling the hole at the center of the fiber [30].

In the present study, we shown how one might address many of the present limitations defined above, challenges that occur during the fabrication of composite materials using the “grinding remelt” protocol. We illustrate how these strategies, with further optimization, could enable a viable route toward the production of ZnSe-doped ChG composite fibers. An As-S-Se chalcogenide glass matrix composition was chosen as the candidate glass composition because of the optical compatibility of sphalerite-type ZnSe in the 3-5 μm range. The ternary ChG composition is shown to provide optimal refractive index match between the glass and crystalline phases, and good crystallization stability. In addition to the compositional attributes of the parent glass matrix, we discuss the thermomechanical and viscoelastic properties of the glass, critical to fiber fabrication considerations, as well as the performance of the parent glass upon preliminary fiberization attempts. As it is critical to the target application where the TM^{2+}:doped ZnSe crystal’s emissive behavior can only be preserved if the dopant remains within the Se-containing crystal lattice and the crystal does not dissolve in the matrix during processing, the dissolution stability of ZnSe within the selected ChG compositions was also examined. Such behavior is challenging to conclusively demonstrate and, to the authors’ knowledge, it has not been thoroughly addressed in prior works. Our efforts examine multiple methods to probe and detect crystal phase stability throughout the material process flow. Here, we specifically highlight the impact of melt temperature and time of synthesis on particle stability, keeping the loading level and the size of particles constant for all experiments. The impact of these variables are quantitatively correlated to the bulk composite’s post-processed properties, using a combination of optical microscopy and second harmonic generation (SHG) as well as the X-ray diffraction (XRD) to assess the physical dispersion of crystals, along with their presence and identity within the composite material.

2. Experimental section

2.1. Glass and composite material synthesis

Candidate ChG matrices were prepared by the melt quenching technique. High purity (5N) sulfur (S), selenium (Se) and arsenic (As)

(from Alfa-Aesar) were stored in a glovebox under controlled atmosphere (H_2O < 1 ppm and O_2 < 0.1 ppm) prior to use for the glass fabrication. Iron (II) chloride, ultra-dry 4N (from Alfa-Aesar) was used for the preparation of a reference Fe^{2+}-doped ChG. The raw materials were introduced in a silica ampoule, which was then sealed under primary vacuum (10^{-2} Torr) with a hydrogen/oxygen torch. Batch materials were subsequently placed in a rocking furnace and heated at a rate of 1℃/min up to 750℃, for a dwell time of 14 h. After dwell, the glasses were air-quenched at 600℃ and annealed at 190℃ for 4 h. ChGs (all made from the same lot of raw elements) were ground using an agate mortar in ambient lab conditions and subsequently sieved with a sieve shaker (DuraTap™ Sieve Shaker, Advantech) with decreasing sieve grid sizes of 125, 53, and 25 μm. Resultant micro-particles with sizes of 25 μm or less were used to prepare composite material. Ground ChG and crystalline powders were mixed in an MBraun glovebox using a loading level of 10 wt% ZnSe particles and introduced in a new silica ampoule. This loading level, while high, was chosen to ensure the presence of crystallites under a wide range of melt conditions and to enable 'detection' of these particles should they be partially 'lost' due to dissolution. After sealing under primary vacuum, the mixture was melted at 550 or 650℃ (dependent upon test) for 1, 8 or 24 h in a rocking furnace. At the end of the synthesis time, the furnace was placed in a vertical position, after which the melt was pulled out and quenched directly using forced air. Subsequently, the composite materials are annealed at 190℃ for 4 h.

Because each powder handling step (grinding, sieving, mixing) resulted in increased moisture content in the resulting post-melted parent glass matrix, handling of powders throughout the composite fabrication was carried out in a dry (N_2-purged) glove box. While cumbersome, this strategy was employed to reduce the exposure time of powders to the ambient lab environment and minimize moisture adsorption. This is critical due to the overlap of mid-IR absorption bands of OH^- and chalcogen-hydride species with the target Fe:ZnSe emission band. The development of a dedicated powder processing and handling protocol will be reported in a future publication [31].

2.2. Base glass material characterization

The coefficient of thermal expansion (CTE), strain point, annealing point and glass transition point were determined by Computer Engineering Service (CES), through dilatometric analysis, using a modified Theta Dilatronic II (Horizontal Furnace) dilatometer, re-engineered by CES to improve accuracy, datalog and analyze all time, temperature and sample displacement data. The 'temperature point' values were determined in a classical fashion, using the intercept of first derivative slopes. The glass sample dimensions used for these measurements were approximately 4 mm in diameter and 50 mm in length. The sample was heated at a rate of 0.5℃/min, with a 2.5g LVDT load applied. A CES-modified, ASTM C1350M-96 beam bending test procedure was used to measure the deflection rate of two Ø3.87 mm × ~50 mm long annealed rods at 235°C. The viscosity of the glass at 440°C was then measured by melting about 40g of glass in a sealed quartz crucible under vacuum using a CES Hi-Temp chalcogenide glass viscometer. After 1h, the vacuum was removed, Ar was introduced at a1 atm leak and the viscometer's quartz spindle shear was measured. The Vogel-Fulcher-Tamman (VFT) equation of the glass was solved in the normal matrix algebra manner, using three measured viscosity values and the corresponding measured temperatures. To render an accurate solution, the difference in viscosity values between the low-end and high-end data points was kept as large as practical. The strain point, annealing point and glass transition point' viscosity values were assigned, by substituting their respective temperatures into the solution of the VFT.

The refractive index of the matrix glass was measured on a Metricon prism coupler (model 2010 M) that has been modified for use in the IR [32]. Prior to the measurement, a reference ZnSe sample was used to calibrate the refractive index of the Ge prism. For each target sample, room-temperature refractive index measurements were conducted ten times and averaged at five IR wavelengths (1.880, 3.300, 4.000, 4.515, and 5.250 μm) to determine the glass' dispersion over this MIR spectral region. The experimental uncertainty of the refractive index measurement is typically on the order of 10^{-4} and is attributable to the spatial compositional and density variations of samples.

Fourier transform infrared (FTIR) transmission data were recorded using a ThermoFisher Nicolet Is5 FTIR spectrometer with a spectral resolution of 4 cm^{-1} and 32 accumulations. Parent glass and composite samples containing glass and crystal powder were both evaluated. Post-sieved ZnSe particle size powder and the as-formed composite were determined by optical microscopy combined with SHG spectroscopy on a custom-built scanning SHG microscope [33] that has been somewhat upgraded. The excitation source used was a 1064 nm picosecond laser (Leukos Opera), which delivers 50 ps pulses at a repetition rate of 1 MHz. The laser incident light was set at an average power of 10 mW and focused into the sample with a near-IR 20 × objective (Mitutoyo M-PLAN APO, NA 0.4), and the resultant SHG at 532 nm was collected in the backward direction using a photomultiplier tube. Large SHG images of 200 × 200 μm^2 (with no polarization analyses) where recorded with a spatial resolution of 0.52 μm. The ZnSe micro-crystals average size has been extracted by measuring the size of particles with ImageJ software [34] on two images. In order to avoid particle aggregation that could lead to false particle sizing, ZnSe particles were dispersed on a microscope slide after ultrasonic processing to reduce aggregation and stirring in an alcohol (ethanol) solution. The image analysis of the dried residue was made after complete evaporation of the solvent.

X-ray diffraction (XRD) data of the parent glass and composite containing crystallites were collected at room temperature, using a PANalytical Empyrean XRD instrument with a beam power of 1.8 kW, a beam wavelength of $\lambda_{Cu\_K\alpha} = 0.15418$ nm, and a beam current of 40 mA at room temperature. The XRD patterns of possible crystalline species were identified using Highscore software and the Joint Committee on Powder Diffraction Standards (JCPDS) PDF files of ZnS blende (No. 005-0566) and ZnSe blende (No. 037-1463). XRD data have been normalized over the intensity value of the most intense peak.

2.3. Fiber drawing

Rod preforms of the parent glass were evaluated for their compatibility with conventional non-oxide glass drawing protocols conducted at the University of Nottingham. Single index rods were used to produce core-only optical fibers, formed using classical preform-to-fiber drawing technique [19]. Both bare fiber (no clad) and polymer clad fibers were produced from single material rods of glass. To attain a fiber with a target diameter of 200 μm, a preform feed rate of 2 mm/min was chosen with a calculated draw speed of 5 m/min. Drawing was stabilized upon a fiber length of 4 m at a draw speed of 4.9 m/min where the diameter stabilized at 200 ± 2 μm. The coating used for the polymer cladding was DeSolite® 3471-3-14 and the UV lamp for the polymerization of the coating was set to full output with the curing chamber N_2-purged at a flow rate of 6 L/min. Fifty six (56) meters of fiber were drawn from a preform of 115 mm in length and a nominal 10 mm outside diameter. The drawing process was performed in a He atmosphere at ambient pressure in a radio frequency (RF) fiber drawing furnace (~70 kHz). The drawing temperature was estimated (from viscosity measurement) to be nominally 280℃ (~10^5 Pa•s). Core diameter and core centricity (within a polymer clad) were assessed using an optical microscope in reflection. The fiber and coating diameters were found to be of 202 ± 5 μm (due to the fractured edge) and 384 ± 5 μm, respectively. Based on the minimum observed coating thickness of 64 ± 4 μm, the fiber was around 27 μm off-center from the initial measurement. Fiber loss of the bare (uncoated) glass fiber was measured using the cutback method [35], on a ~ 10 m in length, ~ 200μm diameter optical fiber, with a Bruker FTIR IF 66 spectrometer; equipped with a Globar light source, KBr beam splitter and MCT detectors cooled with liquid nitrogen.

3. Results

3.1. Choice of candidate base glass composition

In an attempt to minimize the refractive index mismatch between the dopant crystals and the parent matrix, compositional design suggested a mixture of binary arsenic sulfide and arsenic selenide glasses. Fig. 1 shows the calculated refractive indices of As_2S_3, As_2Se_3, ZnSe, along with the measured refractive index of a ternary As_2S_3-As_2Se_3 mixture across the mid-IR spectral window. Room temperature Sellmeier equations for As_2S_3 and As_2Se_3 glasses were provided by IRradiance Glass; the temperature-dependent ZnSe Sellmeier equation used was calculated for room temperature [36]. Calculation of refractive index for the molar glass mixture was a simple linear combination,

$$n_{mix}(\lambda) = 0.946\ n_{As_2S_3}(\lambda) + 0.054\ n_{As_2Se_3}(\lambda) \quad (1)$$

As shown, the blend of two known glass formers in the molar ratio 94.6 As_2S_3 – 5.4 As_2Se_3 provides excellent refractive index matching with ZnSe. This matrix composition was chosen to match the refractive index of the embedded Fe:ZnSe microcrystals with the aim of reducing scattering losses in the 3-5 μm region where the Fe^{2+} active ions in ZnSe emit. Since Fe doping in ZnSe for lasing applications is typically < 0.1 at %, we expect negligible change to the refractive index. This glass composition will be referred to as "base glass" (BG) hereafter.

Fig. 2 illustrates the dilatometric curve of the BG. From this measurement, the temperature values for the strain point (T_s), the conventional annealing point (T_a), the dilatometric glass transition (T_g) and the dilatometric softening point (T_d) were extracted. These values are important, as they are used for the fit of the viscosity curve. The measured coefficient of thermal expansion α(T) from RT to 100℃ and from RT to 175℃ are also extracted. The data for the BG composition are summarized in Table 1. Knowing these parameters is of major importance as strong differences in thermomechanical properties between each component can lead to harmful stress in the final composite material [2], as a result of the different heat treatments experienced during the remelt or the drawing process.

Knowledge of a glass's viscosity behavior identifies the temperature range over which glass can be formed into its final shape. Fig. 3 displays the viscosity curve for the optimized BG as a function of temperature. The use of three viscosity measurements (dilatometer, CES beam bending and CES Hi-Temp Viscometer) at vastly different viscosity ranges enables the precise calculation and extrapolation of the viscosity curve for the base glass, from 150° to 400°C, via a Vogel-Fulcher-Tammann (VFT) fit, following the general expression [37]:

$$\log(\eta) = A + \frac{B}{(T - T_0)} \quad (2)$$

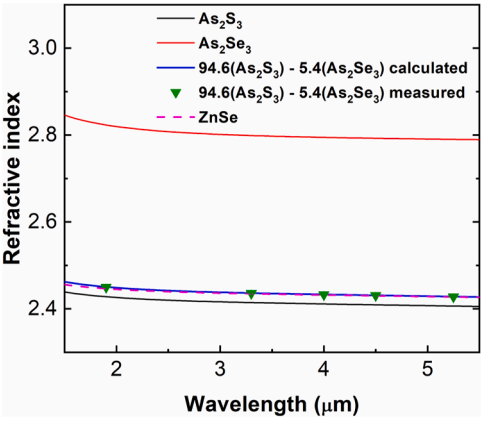

Fig. 1. Refractive indices of As_2S_3, As_2Se_3, ZnSe, and that of a ternary As-S-Se mixture in the mid-IR spectral region.

where *A, B* are empirical material parameters and T_0 is defined as the so-called Vogel divergence temperature. The VFT fit is displayed in the inset of Fig. 3 and the key BG property data are included in the summary of properties for the parent glass matrix in Table 1. The viscosity curve of this base ChG allows us to determine the temperature where it is more appropriate to quench the melt containing ZnSe micro-crystals to ensure their physical dispersion throughout the glass rod, and how that resulting rod could be drawn into fiber. It is desirable that the particles be present in a suitably high volume fraction (loading level by weight %) and be uniformly spread throughout the parent glass volume without agglomeration. Therefore, the glass' viscosity should be fluid enough to allow the microcrystals to disperse, but also high enough that the microcrystals do not settle to the bottom of the melting ampoule at the quenching temperature. Defining this window, these key processing conditions for the candidate ChG matrix composition's melting/quenching protocol, directly impacts the resulting properties of the micro-crystal doped ChG matrix and thus is of critical importance to the resulting composite's optical performance. Moreover, determining the viscosity of a material is also of importance when considering drawing a fiber. The viscosity range to draw good glass fibers typically lies between $10^{4.5}$-$10^{5.5}$Pa•s, which, on the basis of this glass's viscosity curve, corresponds to a temperature between~ 280° and 300°C. This range of drawing temperature matches well with the typical drawing temperatures of As_2Se_3 and As_2S_3 glasses reported to be about 260 and 300°C, respectively [38]. It is important to mention that the introduction of particles in the glass composite may affect the viscosity of the melt but we expect this change may be minimal if the loading level remain low enough.

To understand the potential transmission within both the excitation wavelength regime as well as the mid-IR emission window for Fe:ZnSe doped glass, absorption spectra were compiled for the parent glass and glass where a known amount of Fe was added (as chloride). The parent matrix should exhibit low absorption in both the excitation and emission regions. However, as noted previously, while glass was produced with high purity ingredients, no additional purification was carried out to reduce oxide, moisture of hydride impurities or remaining trace impurities. The purpose for preparing the latter Fe-containing melt was to identify the spectral signature of Fe when introduced in the glass matrix in a controlled manner, illustrating the representative impact of Fe in the glass matrix, were it to diffuse from the doped crystal (Fe:ZnSe). This signature might be expected for example, if the TM diffused from the active crystal during its partial or full dissolution. Fig. 4a presents the IR absorption coefficient of the BG with and without iron impurities. The classical absorption spectrum of Fe^{2+} in ZnSe crystal at room temperature and its emission band at 77 K, centered around 4 μm and corresponding to $^5T_2 \rightarrow {}^5E$ transition, are also displayed for comparison. The as-melted, 'unpurified' parent base glass exhibits good IR optical transparency up to its multi-phonon limit at~ 900 cm^{-1} (~ 11 μm). Fig. 4b shows the fiber loss (in dB/m) measured on the un-coated single index BG optical fiber. Well-known extrinsic absorption bands associated with hydrogen and oxygen impurities can be observed in both spectra. These absorption bands correspond to vibrational modes of: -S-H at 4880 cm^{-1} (2.05 μm), 2740 cm^{-1} (3.65 μm) and 2480 cm^{-1} (4 μm); -O-H^- at 3420 cm^{-1} (2.92 μm); -Se-H at 2430 cm^{-1} (4.12 μm); -As-H at 1990 cm^{-1} (5.02 μm); H_2O at 1590 cm^{-1} (6.3 μm); -As-O at 1130 cm^{-1} (8.9 μm) and 1050 cm^{-1} (9.5 μm); and finally -Se-O at 940 cm^{-1} (10.1 μm) [27]. The addition of 100 ppm (in atomic percent) of iron (II) in the As-S-Se base glass results in a strong increase of the overall losses in the IR, without the observation of an additional absorption peak.

3.2. ZnSe dissolution in base glass

The fabrication of a stable optical composite fiber that emits in the desired mid-IR spectral region requires that the dopant crystal remains stable in its particle form, during both glass melting and fiber formation.

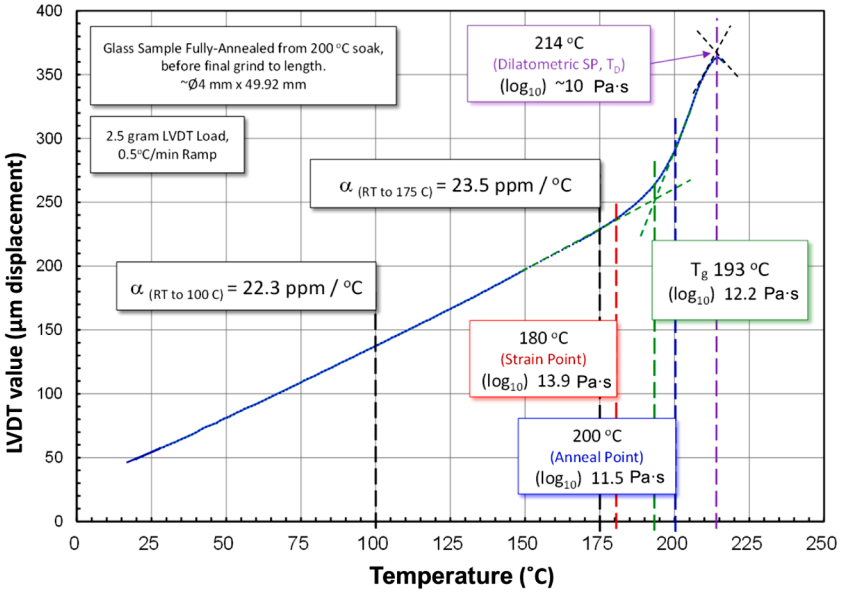

Fig. 2. Thermomechanical dilatometry curve of the base chalcogenide glass as a function of temperature.

Table 1
Thermal and thermomechanical data of the BG composition (94.6 As_2S_3 – 5.4 As_2Se_3), including VFT coefficients (see Eq. (2)).

T_s (C)	T_a (C)	T_g (C)	T_d (C)	$\alpha_{(RT\ to\ 100C)}$ (ppm/C)	$\alpha_{(RT\ to\ 175C)}$ (ppm/C)	A	B	T_0 (C)
180	200	193	214	22.3	23.5	-8.32	3602	17.82

To assess this stability and to differentiate the target crystal from the surrounding matrix and any possible other crystalline phases that might form during the processing steps, XRD was employed on the parent glass following incorporation of a fixed volume fraction of similar sized crystallites, and subjected to various processing steps. While other efforts to process composite media similar to that shown in this work have been published previously [5,23,39], no systematic delineation of particle stability has so far been carried out, specifically looking for the formation of similar phases that can result from dissolution/recrystallization processes.

Fig. 5a presents the XRD experimental data of ZnS and ZnSe crystals that are displayed for comparison. Fig. 5b illustrates the XRD data of the BG and ZnSe-doped BG after remelt at 650℃ for different dwell times (1, 8 and 24 h). In these studies, ground ZnSe (not containing Fe) was added to the ground parent glass matrix, mixed, (re-) melted, quenched and analyzed. One can see that the resulting composite materials, after 1 and 8 h of synthesis at this temperature, show XRD peaks corresponding to ZnS and ZnSe crystals (patterns corresponding to JCPDS data files of ZnS Blende No. 005-0566 and ZnSe Blende No. 037-1463) and that no XRD lines can be observed for the undoped BG showing its amorphous state. It is important to note on Fig. 5b that after 24 h of remelt only ZnS diffraction peaks remain. With increasing time of remelt, the relative intensity of ZnSe crystals peaks decreases with a concurrent increase to the peak seen for ZnS. This effect was seen repeatedly under a range of melt times and compositions. While keeping the time of synthesis constant, the same tendency is observed in Fig. 5c,d where the relative intensity of XRD peaks from ZnSe crystals decreases to the profit of ZnS

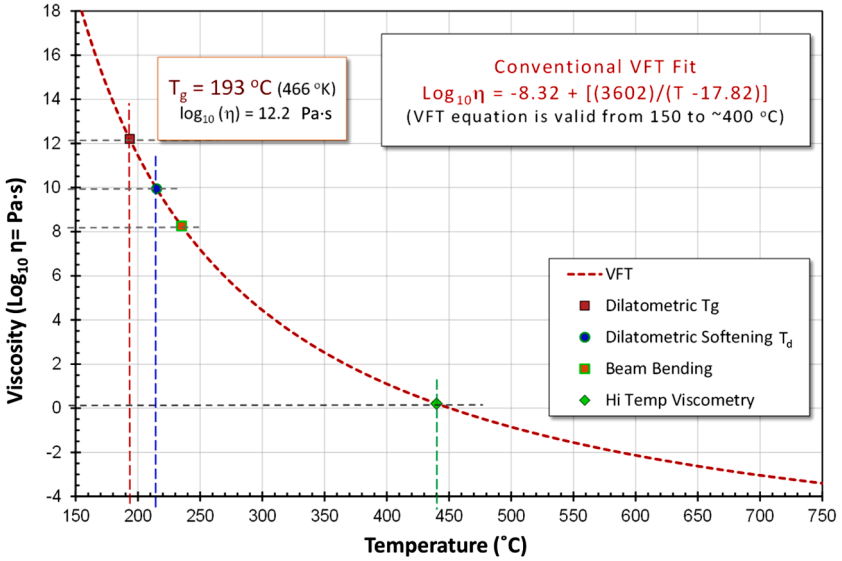

Fig. 3. Viscosity curves in function of temperature of the chalcogenide base glass using a VFT fit.

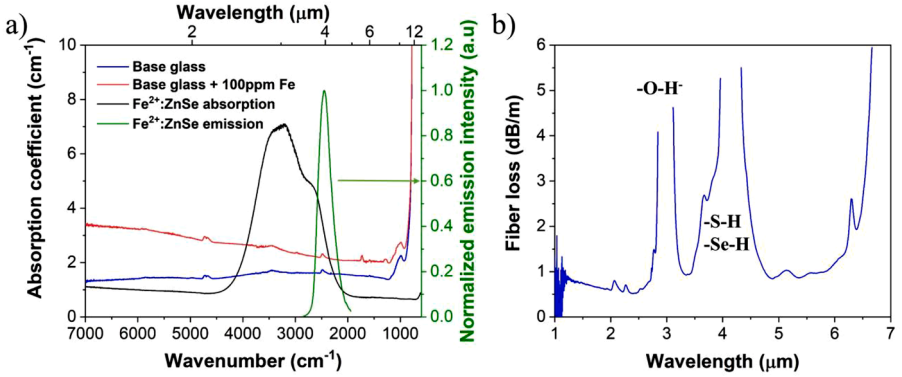

Fig. 4. a) Absorption coefficient of BG with and without iron doping with the absorption and the mid-IR emission bands for Fe^{2+} in ZnSe crystals at 77K; b) IR fiber loss of BG optical fiber

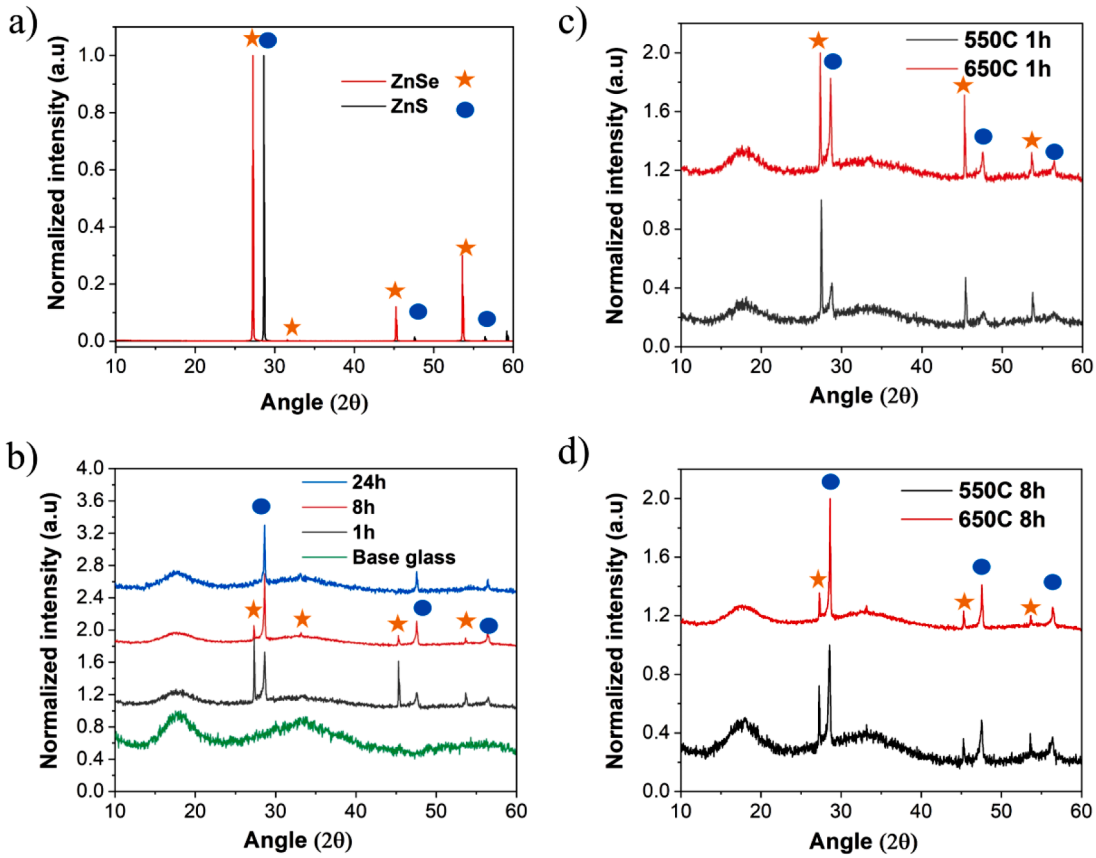

Fig. 5. XRD data of a) ZnSe and ZnS crystals, b) ZnSe-doped BG melted at 650℃ for 1, 8 and 24 h, c) ZnSe-doped BG melted at 550 and 650℃ for1 h and d) ZnSe-doped base glassesBG melted at 550 and 650℃ for 8 h. Diffractograms on graphs b), c) and d) were vertically shifted for clarity.

with the increase in temperature of synthesis. As one might expect, the increase in temperature serves to increase the rate of dissolution and formation of the more stable ZnS phase. This is visible in Fig. 5c with the increase in intensity of peaks corresponding to the ZnS blende, and in Fig. 5d with the decrease in intensity of ZnSe diffraction peaks. Similar findings were obtained when the dopant was introduced to both of the binary materials, As_2S_3, As_2Se_3 and an alternative GeSbS composition (data not shown). These data conclusively show that ZnSe crystals disintegrate during the remelt process and that both the time and the temperature of synthesis have an impact on it.

In order to define a possible low temperature limit to ZnSe dissolution, Fig. 6 shows the diffraction data obtained on a composite material made of ZnSe and BG powders that have been heated at 360℃ for 30 min in an ampoule under Ar at 1 atm. For comparison, the experimental XRD pattern of ZnSe powders is also displayed. The diffraction data of the composite material only reveal the presence of cubic ZnSe crystals and the absence of ZnS or any other crystal phases. This finding, while useful as a lower boundary does not result in glass with sufficient homogeneity to yield desirable optical fiber.

While XRD provides direct evidence of what crystalline phases withstand the remelt protocols used, it is desirable to have a non-destructive means of seeing and assessing the presence of the crystalline phase(s) of interest. An alternative method to evaluate the presence of ZnSe in powder mixtures (ZnSe alone and mixed with BG) was applied that exploits the unique linear and nonlinear optical properties of the composite ingredients using a combination of optical and SHG micro-

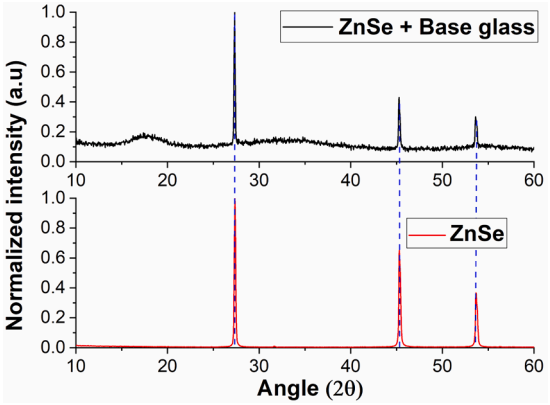

Fig. 6. XRD data of (top) ZnSe mixed with BG powders after heat treatment at 360C for 30 min and (bottom) reference spectra for ZnSe powders.

scopy. Fig. 7 shows overlaid bright-field and SHG images obtained from the post-sieved ZnSe powders alone and from the surface of one of the composite materials after melting at 650C for 8 h. The largest measured particle for the sieved ZnSe powders had a size of~ 24 μm, close to the expect 'fines' passing through the 25 μm sieve grid, while bigger particles (up to~ 32μm) can be observed on the surface of ZnSe-doped BG after remelt at 650C for 8 h. The measured average particle size of the ZnSe powders after grinding and sieving is of 4.8 μm, with a majority of particles having a size between 2.5 and 3.5 μm. The same batch of post-ground ZnSe powders were those used in the remelt fabrication protocol used for the composite material synthesis. It is interesting to see that there exists an excellent overlap between the measured SHG signal and the darker areas within the bright-field images. The small positional shift observed is likely due to the effect of weak mechanical vibrations in the experimental setup, as the bright-field and SHG images are taken sequentially. In complement to optical microscopy, SHG microscopy provides a powerful means to examine the nonlinear optical (NLO) responses of species in homogeneous or composite media. Under the action of an intense light (*e.g.*, pulsed lasers), the SHG response obtained from a material is characterized by the second-order nonlinear susceptibility $\chi^{(2)}$ which depends intrinsically on the crystal symmetry of the material [40]. Hence, in order for a material to have a measurable SHG response, it needs to be non-centrosymmetric (*i.e.*, to have $\chi^{(2)} \neq 0$). In contrast, isotropic materials are centrosymmetric and thus are not SHG-active ($\chi^{(2)} = 0$). It can be seen that contrary to optical microscopy, SHG selectively detects the presence of ZnS/ZnSe crystals, contrasting those features from the glassy matrix as well as from other species (i.e., extrinsic defects such as dust or other surface imperfections such as polishing defects). The distinction results from the fact that in normal conditions, a glassy material does not exhibit a NLO response due to its centrosymmetric structure [41,42]. Conversely, ZnSe and ZnS crystals with their zinc blende structures are non-centrosymmetric and thus are both SHG-active [43,44]. It is thus possible to link and ascribe those areas to ZnS/ZnSe micro-crystals. In addition, the magnitude of such SHG response could allow to differentiate between ZnS and ZnSe crystal type, due to the difference in their second-harmonic coefficient $|d|$(pm/V)) (where $|d| = \frac{1}{2}|\chi^{(2)}|$ following convention II [45]) between ZnS and ZnSe that are equal to 8 and 30pm/V at 1321 nm respectively ($|d|_{ZnS} < |d|_{ZnSe}$) [43]. However, that would require another technique to validate this protocol as many factors could influence on the measurement as, for instance, the thickness of the particles at the surface after the sample polishing. In a future study, we project to further combine the current optical/SHG microscopy functionalities with Raman spectroscopy in order to spectrally discriminate between ZnS and ZnSe embedded micro-particles.

4. Discussion

As depicted in Fig. 1 the optimized composition 94.6 As_2S_3 – 5.4 As_2Se_3 has a refractive index compatible with that of a ZnSe crystal in the 3-5μm spectral range, which is the region of interest for the luminescence of Fe^{2+} in a tetrahedral configuration. This should enable one to reduce the losses due to scattering in the composite material and, by extension, in the final optical fiber. We demonstrate that this glass composition exhibits very good fiber draw characteristics, without presenting visible signs of crystallization during the drawing process. Although the resultant optical fiber exhibits high losses, (for the most part, assigned to the unpurified elements used in the synthesis of the preform), the fiber transmits light in the IR up to~ 6 μm. The data presented in Fig. 4 underscore the belief that impurity bands present in the BG preform translate directly to the fiber following fabrication. Additionally, the data illustrate the role of impurity content (both extrinsic and intrinsic) on loss in the key spectral region of Fe:ZnSe emission, and that subsequent matrix purification will likely be required to ensure low loss in the regions where emission occurs. Previous work by our team and others has shown that purification protocols can dramatically reduce impurities in these types of bulk glass and fibers, impacting both optical properties [46] and mechanical properties [47]. Meanwhile, this glass composition has shown to be a particularly suitable candidate for the fabrication of Fe:ZnSe/ChGs composite fibers.

In order to optimize the melting temperature of the ZnSe + BG powders mixture, it is crucial to know the viscosity of the glass melt. Having this knowledge enables one to optimize the melting conditions that ensure a good homogenization of the melt and reduce the risks of particles' sedimentation before and during the quenching. The goal is to have suitably long melt times at high temperature to ensure

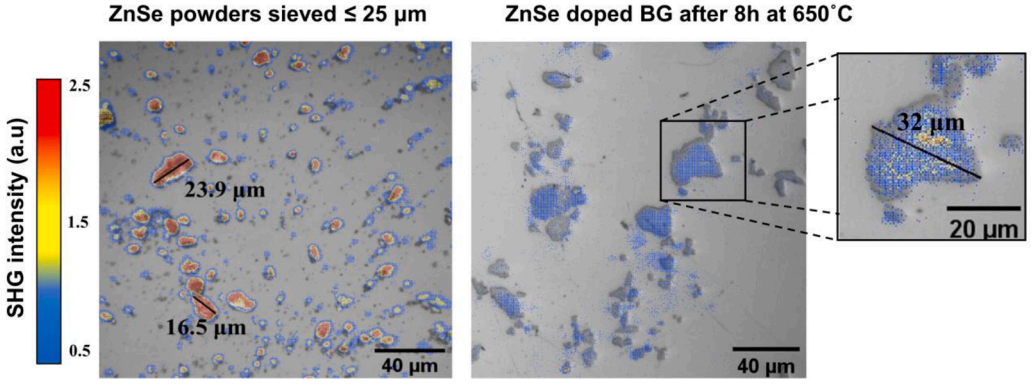

Fig. 7. Combined optical microscopy and SHG images (left) of post-sieved ZnSe particles passing through a 25μm sieve, on a microscope slide and (right) SHG map (dots) representative of ZnS/ZnSe particles in a ZnSe doped As-S-Se base glass after remelt for 8 h at 650C of the mixture. The scale bar and drawn lines illustrate the length scale of the features shown. The colors of the regions are representative of the SHG intensity.

compositional uniformity leading to optical (index) homogeneity. This processing condition opposes the condition where the dopant powder sees a melt environment in which it remains intact, not dissolving or decomposing with time and/or temperature. Hence, an optimal condition would be to subject the powder to short a time, at as low a temperature possible, to enable good physical dispersion in a fluid melt, with no physical degradation. Except for the glass melted a 550°C for 1h, glasses obtained from the remelt of base glass powders alone (not presented) do not exhibit signs of trapped bubbles. This temperature coincides with a viscosity value of $\sim 10^{-1.5}$ Pa•s. After 8 h of synthesis at 550℃, the glass is bubble-free without evidence of visible striae indicating that temperature limit is indeed the viscosity limit below which the viscosity increases drastically. Hence, at lower temperatures, the 'melt' becomes too viscous to ensure a good melt homogenization and to allow for the evacuation of the bubbles. Thus, 550 ℃ for 1 h defines a lower limit condition for this material.

The observation of ZnS diffraction peaks for the composite materials strongly suggests that ZnSe crystals are either dissolved or converted into ZnS during the remelt process. The formation of ZnS crystals can be explained by the fact that the liquid melt media within which the particles are dispersed, is composed mainly of sulfur (94.6 As_2S_3 – 5.4 As_2Se_3). It can also be interpreted through the analysis of the standard enthalpy of formation of sphalerite-type ZnS ($\Delta_f H^0$ ZnS (298 K) = -201.07 ± 1.3 kJ mol^{-1} [48]) that is lower than that of sphalerite-type ZnSe ($\Delta_f H^0$ ZnSe (298 K) = - 164 kJ mol^{-1} [49]), with a lower enthalpy suggests enhanced formation and stability. Meanwhile, considering the high melting temperature of ZnSe (1522 ± 2℃ [49]) one would expect that the particle survives during the remelt process using low melting temperature and short dwell time. However, this is not the case, even for a sample that underwent a remelt for 1 h at 550°C, as evidenced by the observation of ZnS diffraction peaks in Fig. 5c. The disintegration of ZnSe particles during the synthesis of the composite material has already been pointed out in prior results [3]. This explanation is proposed as the reason why Fe/Cr:ZnSe doped As-S-Se composite materials do not show any luminescence in the mid-IR.

It is important to mentioned that ZnSe dissolution has also been obtained intentionally in As-S glasses in order to make a ZnS-doped chalcogenide glass ceramic [26,50]. However, this was achieved through a melting/quenching in water protocol following processing at much higher temperatures (900-950℃) than the remelt temperature used here. In any case, to have a laser that emits in the 3-5 μm range, the Fe^{2+} ions must remain integrated in the ZnSe (lattice) particles and not in ZnS where the emission band is shifted to (a measurably) lower wavelength (2-4 μm). Additionally, it is undesirable to for the dopant to be in the chalcogenide glass where other oxidation states may be present. Thus, it is essential to suppress the dissolution of Fe:ZnSe crystals, in order to avoid (i) the loss of Fe:ZnSe luminescent active crystals (through their dissolution) and (ii) the detrimental impact of iron leaving the crystal that can induce strong absorption losses (as observed on Fig. 4a) in the mid-IR, especially in As-S-Se chalcogenide glasses. The losses due to iron in ChGs could be reduced by changing the glass matrix (i.e., using Ge-Se, Ge-Se-Te, Ge-Sb-Se or Ge-As-Se compositions), due to their better capacity to dissolve iron [51]. However, the use of these glass hosts with refractive indices substantially different from those of ZnSe crystals would be expected to lead to scattering losses in the final optical fiber.

Two mechanisms can be proposed to explain the undesirable formation of ZnS micro-crystals in this study. The first is a simple dissolution and re-crystallization process, whereby ZnSe are dissolved in favor of ZnS crystallization and growth. The second is conversion of ZnSe into ZnS by diffusion and substitution of selenium by sulfur. The former mechanism would imply the presence of a ZnSSe intermediate crystalline phase. An argument against this mechanism is the absence of diffraction peaks for such an intermediate phase, supporting the theory that the process involved is more likely to be due to ZnSe micro-crystals' dissolution during the remelt process and a crystallization of ZnS particles. Moreover, in the latter mechanism, one would expect that the size of the particles remains constant or even decreases as the molar volume of ZnS (~ 23.8 $cm^3.mol^{-1}$) is smaller than that of ZnSe (~ 27.4 $cm^3.mol^{-1}$). Nevertheless, after 8 h of remelt at 650℃, micro-crystals of 34 μm, with a size well above the initial ZnSe particle size (≤ 25 μm), were observed by optical/SHG microscopy (Fig. 7). These facts strongly suggest that ZnSe particles are dissolved during the remelt process and that cubic ZnS micro-crystals crystallize in the glass melt despite the low temperature (550℃) or the short time of synthesis (1 h) used to prevent the initial ZnSe dissolution.

Alternative routes of synthesis can be envisioned to minimize this instability. Specifically, the use of a hot-press has been proposed to make ZnSe-doped composite materials [3]. The use of such a process could reduce the temperature required to make the composite. As discussed previously, ZnSe particles are dissolved even at a temperature as low as 550℃. It would be interesting to learn if the particles remain intact after exposure to a temperature near to the one used during the hot pressing of the powders (350-410℃). Moreover, as this temperature is close to the drawing temperature of the BG (~ 280℃ using the classic preform to fiber drawing technique and ~ 320℃ with the crucible drawing method), this test may lend insight to the vulnerability of ZnSe during the drawing process. Indeed, as depicted in Fig. 6, after being heated at 360℃ for 30 min, the resulting material did not exhibit ZnS diffraction peaks, while ZnSe XRD lines remained. Recognizing the need for further experimentation, this observation illustrates that the use of a hot press could be envisioned in the manufacture of the composite material and a preform, by mitigating the risk for excessive ZnSe dissolution and/or sublimation. The same outcome could occur during the drawing process. An additional method presently being evaluated by our team presently involves the use of a sacrificial protective shell, which allows the active particle to survive the melt conditions needed to form stable, homogeneous glass. The results of these efforts will be reported in future publications.

5. Conclusion

In an effort to produce a composite fiber laser comprised of active Fe:ZnSe crystals in a glass matrix that emits in the 3-5 μm mid-IR region, a ChG matrix of composition 94.6 As_2S_3 – 5.4 As_2Se_3 has been developed successfully and its properties have been quantified. The designed As-S-Se base glass has been shown to have a refractive index which matches that of sphalerite-type Fe:ZnSe micro-crystals. The transmission window of the glass and the optical fiber (to date, without further purification) has been shown to be compatible with the luminescence expected in the spectral range of Fe^{2+} in ZnSe. However, the elements will need to be further purified (by distillation of sulfur and selenium, and sublimation of arsenic) in order to avoid the absorption (due to vibrational modes of extrinsic impurities) of the photons emitted by the active ions in the mid-IR. The BG' thermomechanical and viscoelastic properties have been investigated and quantified, providing valuable information that enabled optimizing the fiber drawing temperature and the melting conditions required for the Fe:ZnSe-doped composite material synthesis using the grinding remelt technique. XRD analysis of the BG, dopant crystal phase and post-melted, remelted composite revealed the presence of ZnS diffraction peaks under specific melting conditions, indicative of a proposed ZnSe dissolution and ZnS recrystallization process. We believe that the driving force behind the ZnSe dissolution and the formation of ZnS crystals is likely the difference in formation energies between the two phases.

The use of a new tool that combines optical microscopy and SHG allows the non-destructive observation of crystalline particles in the matrix glass, providing a means to identify possible particle agglomeration and/or crystallite particle growth, with processing. The ability to differentiate between crystalline phases (ZnSe or ZnS) has yet to be conclusively shown. XRD data were able to document the absence of a putative intermediate ZnSSe phase. With this absence of ZnSSe diffraction peaks, we conclude that the mechanism involved is likely due to a

ZnSe micro-crystals dissolution followed by a reaction of the zinc with the excess of sulfur in the melt, which leads to the crystallization of ZnS micro-crystals. This model is at odds with another mechanism that would imply a progressive substitution of sulfur by selenium in the micro-crystals. Meanwhile, ZnSe dissolution test at a very low temperature did not reveal any sign of ZnS formation. This constitute a promising avenue where the use of a some form of a passivation layer to mitigate (slow or eliminate) the dissolution of ZnSe, could prove helpful in creating a Fe:ZnSe/ChG composite fiber. How this translates to the creation of an active medium where the Fe:ZnSe emission is preserved for use as a fiber laser, remains under investigation.

CRediT authorship contribution statement

Matthieu Chazot: Conceptualization, Methodology, Investigation, Validation, Writing - original draft, Visualization, Supervision. **Chanelle Arias:** Methodology, Investigation, Writing - original draft. **Myungkoo Kang:** Methodology, Investigation, Writing - review & editing, Supervision. **Cesar Blanco:** Methodology, Investigation. **Alexandros Kostogiannes:** Methodology, Investigation. **Justin Cook:** Formal analysis, Investigation. **Anupama Yadav:** Investigation, Supervision. **Vincent Rodriguez:** Methodology, Investigation, Writing - review & editing. **Frederic Adamietz:** Methodology, Investigation. **Dominique Verreault:** Methodology, Investigation, Writing - review & editing. **Sylvain Danto:** Methodology, Investigation, Writing - review & editing. **Thomas Loretz:** Methodology, Investigation, Writing - review & editing. **Angela Seddon:** Conceptualization, Visualization, Writing - review & editing. **David Furniss:** Methodology, Investigation. **Kenneth Schepler:** Conceptualization, Methodology, Formal analysis, Writing - review & editing, Project administration, Funding acquisition. **Martin C. Richardson:** Conceptualization, Project administration, Funding acquisition. **Kathleen A. Richardson:** Conceptualization, Methodology, Formal analysis, Writing - review & editing, Supervision, Project administration, Funding acquisition.

Declaration of Competing Interest

The authors declare that they have no known competing financial interests or personal relationships that could have appeared to influence the work reported in this paper.

Acknowledgment

The authors thank the financial support of AFOSR for the Grant FA9550-19-1-0127. This work was partially supported by the University of Central Florida under the Pre-eminent Postdoctoral Program (P^3). VR and DV thanks financial support from the French National Research Agency (ANR) in the framework of the "Investments for the Future" Programme IdEx Bordeaux LAPHIA (ANR-10-IDEX-03-02).

References

[1] B.J. Eggleton, B. Luther-Davies, K. Richardson, Chalcogenide photonics, Nat Photonics 5 (2011) 141–148, https://doi.org/10.1038/nphoton.2011.309.
[2] S.D. Jackson, R.K. Jain, Fiber-based sources of coherent MIR radiation : key advances and future prospects (invited), Opt Express 28 (21) (2020) 30964, https://doi.org/10.1364/OE.400003.
[3] A. Yang, J. Qiu, J. Ren, et al., 1.8–2.7 μm emission from As-S-Se chalcogenide glasses containing ZnSe: Cr 2+ particles, J Non Cryst Solids 508 (January) (2019) 21–25, https://doi.org/10.1016/j.jnoncrysol.2019.01.007.
[4] E.V. Karaksina, L.A. Ketkova, M.F. Churbanov, E.M. Dianov, Preparation of Mid-IR-Active As2S3/ZnS(ZnSe):Cr2+ composites, Inorg Mater 49 (3) (2013) 223–229, https://doi.org/10.1134/S0020168513030072.
[5] D.V. Martyshkin, J.T. Goldstein, V.V. Fedorov, S.B. Mirov, Crystalline Cr2+:ZnSe/chalcogenide glass composites as active mid-IR materials, Opt Lett 36 (9) (2011) 1530–1532, https://doi.org/10.1364/OL.36.001530.
[6] L. Isaenko, A. Yelisseyev, A. Tkachuk, et al., Crystalline laser and nonlinear optical materials for the mid-IR, in: M Ebrahim-Zadeh, IT Sorokina (Eds.), Mid-Infrared Coherent Sources Appl, eds., Springer Science + Business Media B.V, 2008, pp. 3–168.
[7] M. Kang, L. Sisken, C. Lonergan, et al., Monolithic Chalcogenide Optical Nanocomposites Enable Infrared System Innovation: Gradient Refractive Index Optics, Adv Opt Mater 8 (10) (2020) 24–27, https://doi.org/10.1002/adom.202000150.
[8] M. Kang, L. Sisken, J. Cook, et al., Refractive index patterning of infrared glass ceramics through laser-induced vitrification [Invited], Opt Mater Express 8 (9) (2018) 2722, https://doi.org/10.1364/ome.8.002722.
[9] J. Ren, X. Lu, C. Lin, R. Jain, Luminescent ion-doped transparent glass ceramics for mid-infrared light sources, Opt Express 28 (15) (2020) 21522–21548, https://doi.org/10.1364/oe.395402.
[10] J.W. Evans, T.R. Harris, B.R. Reddy, K.L. Schepler, P.A. Berry, Optical spectroscopy and modeling of Fe2+ ions in zinc selenide, J Lumin 188 (February) (2017) 541–550, https://doi.org/10.1016/j.jlumin.2017.04.017.
[11] J. Kernal, V.V. Fedorov, A. Gallian, S.B. Mirov, V.V. Badikov, 3.9-4.8 μm gain-switched lasing of Fe : ZnSe at room temperature, Opt Express 13 (26) (2005) 10608–10615, https://doi.org/10.1364/OPEX.13.010608.
[12] V.V. Fedorov, S.B. Mirov, A. Gallian, et al., 3.77-5.05-μm tunable solid-state lasers based on Fe2+-doped ZnSe crystals operating at low and room temperatures, IEEE J Quantum Electron 42 (9) (2006) 907–917, https://doi.org/10.1109/JQE.2006.880119.
[13] S. Mirov, V. Fedorov, New Regimes of Excitation and Mid-IR Lasing of Transition Metal Doped II–VI Crystals, in: M Ebrahim-Zadeh, IT Sorokina (Eds.), Mid-Infrared Coherent Sources Appl, eds., Springer, 2008, pp. 261–314.
[14] J. Ballato, E. Snitzer, Fabrication of fibers with high rare-earth concentrations for Faraday isolator applications, Appl Opt 34 (30) (1995) 6848–6854.
[15] S. Jackson, R. Vallé, M. Bernier, Chalcogenide glasses for mid-infrared fibers, Elsevier, 2020 ed. Mid-Infrared Fibers. to appear in Elsevier eds.
[16] T. Kanamori, Y. Terunuma, S. Takahashi, T. Miyashita, Chalcogenide Glass Fibers for Mid-Infrared Transmission, J Light Technol 2 (5) (1984) 607–613, https://doi.org/10.1109/JLT.1984.1073657.
[17] M. Chazot, M. El Amraoui, S. Morency, A. Hanafi, Y. Messaddeq, V. Rodriguez, Thermal characterizations and investigation of the drawing region in Ge-As-S glasses for IR optical fibers, J Non Cryst Solids (2019), https://doi.org/10.1016/j.jnoncrysol.2018.12.022.
[18] M.F. Churbanov, V.S. Shiryaev, I.V. Scripachev, et al., Optical fibers based on As-S-Se glass system, J Non Cryst Solids 284 (1–3) (2001) 146–152, https://doi.org/10.1016/S0022-3093(01)00394-5.
[19] M. Chazot, M. El Amraoui, S. Morency, Y. Messaddeq, V. Rodriguez, Investigation of the drawing region in the production of Ge-S-I optical fibers for infrared applications, J Non Cryst Solids 476 (2017), https://doi.org/10.1016/j.jnoncrysol.2017.09.037.
[20] E.V. Karaksina, V.S. Shiryaev, L.A. Ketkova, Preparation of composite materials for fiber optics based on chalcogenide glasses containing ZnS(ZnSe):Cr(2+) crystals, J Non Cryst Solids 377 (2013) 220–224, https://doi.org/10.1016/j.jnoncrysol.2012.12.021.
[21] E.V. Karaksina, R.A. Mironov, R.M. Shaposhnikov, L.A. Ketkova, The composite materials on the basis of As2S3 glass containing crystals ZnS and ZnS doped with Cr(2+), J Optoelectron Adv Mater 13 (11–12) (2011) 1433–1436.
[22] S.B. Mirov, V.V. Fedorov, D.V.. Martyshkin, I.S. Moskalev, M.S. Mirov, V. P. Gapontsev, Progress in mid-IR Cr2+ and Fe2+ doped II-VI materials and lasers, Opt Mater Express 1 (5) (2011) 898, https://doi.org/10.1364/OME.1.000898.
[23] R.A. Mironov, E.V. Karaksina, A.O. Zabezhailov, R.M. Shaposhnikov, M. F. Churbanov, E.M. Dianov, Mid-IR luminescence of Cr 2+ : II - VI crystals in chalcogenide glass fibres, Quantum Electron 40 (9) (2010) 828–829, https://doi.org/10.1070/QE2010v040n09ABEH014408.
[24] X. Lu, J. Li, L. Yang, et al., Broadband mid-infrared (2.5–5.5 μm) emission from Co 2+ /Fe 2+ codoped chalcogenide glass ceramics, Opt Lett 45 (9) (2020) 2676, https://doi.org/10.1364/ol.392190.
[25] X. Lu, R. Zhang, Y. Zhang, et al., Crystal-field engineering of ultrabroadband mid-infrared emission in Co2+-doped nano-chalcogenide glass composites, J Eur Ceram Soc 40 (1) (2020) 103–107, https://doi.org/10.1016/j.jeurceramsoc.2019.09.006.
[26] X. Lu, Z. Lai, R. Zhang, et al., Ultrabroadband mid-infrared emission from Cr 2+ -doped infrared transparent chalcogenide glass ceramics embedded with thermally grown ZnS nanorods, J Eur Ceram Soc 39 (11) (2019) 3373–3379, https://doi.org/10.1016/j.jeurceramsoc.2019.04.048.
[27] G.E. Snopatin, V.S. Shiryaev, V.G. Plotnichenko, E.M. Dianov, M.F. Churbanov, High-purity chalcogenide glasses for fiber optics, Inorg Mater 45 (13) (2009) 1439–1460, https://doi.org/10.1134/S0020168509130019.
[28] S.C. MGC Aro Jr., S.A. McDaniel, et al., Continuous wave Fe 2 + : ZnSe mid-IR optical fiber lasers, Opt Express 28 (20) (2020) 30263–30274.
[29] J.R. Sparks, R. He, N. Healy, et al., Zinc selenide optical fibers, Adv Mater 23 (14) (2011) 1647–1651, https://doi.org/10.1002/adma.201003214.
[30] A.T. Hendrickson, S.C. Aro, J.R. Sparks, et al., Post-processing ZnSe optical fibers with a micro-chemical vapor transport technique, Opt Mater Express 10 (12) (2020) 3125–3136.
[31] A. Kostogiannes, Powder optimization study towards the production of ZnSe -doped As-S-Se composite materials. to be Publ, 2021.
[32] B. Gleason, K. Richardson, L. Sisken, C. Smith, Refractive Index and Thermo-Optic Coefficients of Ge-As-Se Chalcogenide Glasses, Int J Appl Glas Sci 7 (3) (2016) 374–383, https://doi.org/10.1111/ijag.12190.
[33] G. Gouget, M. Duttine, E. Durand, A. Villesuzanne, V. Rodriguez, Isolating the Two Room-Temperature Polymorphs of NaNbO 3 : Structural Features, Optical Band Gap, and Reactivity, 2019, https://doi.org/10.1021/acsaelm.8b00125.
[34] C.A. Schneider, W.S. Rasband, K.W. Eliceiri, NIH Image to ImageJ: 25 years of image analysis, Nat Methods 9 (7) (2012) 671–675, https://doi.org/10.1038/nmeth.2089.

[35] Z. Tang, V.S. Shiryaev, D. Furniss, et al., Low loss Ge-As-Se chalcogenide glass fiber, fabricated using extruded preform, for mid-infrared photonics, Opt Mater Express 5 (8) (2015) 1722–1737, https://doi.org/10.1364/OME.5.001722.
[36] William J. Tropf, Temperature-dependent refractive index models of BaF2, CaF2, MgF2, SrF2, LiF, NaF, KCl, ZnS, and ZnSe, Opt Eng 34 (5) (1995) 1369–1373.
[37] J. Rault, Origin of the Vogel-Fulcher-Tammann law in glass-forming materials: The β Bifurcation, J Non Cryst Solids 271 (3) (2000) 177–217, https://doi.org/10.1016/S0022-3093(00)00099-5.
[38] D.S. Deng, J.-C. Nave, X. Liang, S.G. Johnson, Y. Fink, Exploration of in-fiber nanostructures from capillary instability, Opt Express 19 (17) (2011) 16273, https://doi.org/10.1364/oe.19.016273.
[39] E.V. Karaksina, L.a. Ketkova, M.F. Churbanov, E.M. Dianov, Preparation of mid-IR-active As2S3/ZnS(ZnSe):Cr2+ composites, Inorg Mater 49 (3) (2013) 223–229, https://doi.org/10.1134/S0020168513030072.
[40] Rodriguez V., Sciences U.F.R., Université C. Introduction au techniques de caractérisation des molécules et matériaux en optique non linéaire quadratique. n. d.
[41] A. Lepicard, F. Adamietz, V. Rodriguez, K. Richardson, M. Dussauze, Demonstration of dimensional control and stabilization of second harmonic electro-optical response in chalcogenide glasses, Opt Mater Express 8 (6) (2018) 1613, https://doi.org/10.1364/ome.8.001613.
[42] A. Lepicard, F. Bondu, M. Kang, et al., Long-lived monolithic micro-optics for multispectral GRIN applications, Sci Rep 8 (7388) (2018) 1–8, https://doi.org/10.1038/s41598-018-25481-x.
[43] H. Wagner, M. Kühnelt, W. Langbein, J. Hvam, Dispersion of the second-order nonlinear susceptibility in ZnTe, ZnSe, and ZnS, Phys Rev B 58 (16) (1998) 10494–10501, https://doi.org/10.1103/PhysRevB.58.10494.
[44] H. Komine, W.H. Long, J.W. Tully, E.A. Stappaerts, Quasi-phase-matched second-harmonic generation by use of a total-internal-reflection phase shift in gallium arsenide and zinc selenide plates, Opt Lett 23 (9) (1998) 661, https://doi.org/10.1364/ol.23.000661.
[45] Kuzyk M.G., Dirk C.W. Characterization Techniques and Tabulations for Organic Nonlinear Optical Materials. 1998.
[46] A.N.Y. Adav, M.Y.K. Ang, C. Laudia, et al., Impact of raw material surface oxide removal on dual band infrared optical properties of As 2 Se 3 chalcogenide glass, Opt Mater Express 10 (9) (2020) 2274–2288.
[47] S. Danto, M. Dubernet, B. Giroire, et al., Correlation between native As2Se3 preform purity and glass optical fiber mechanical strength, Mater Res Bull 49 (1) (2014) 250–258, https://doi.org/10.1016/j.materresbull.2013.08.004.
[48] V.O. Osadchii, M.V. Fedkin, E.G. Osadchii, Electrochemical determination of the thermodynamic parameters of sphalerite, ZnS, J Alloys Compd. 636 (2015) 368–374, https://doi.org/10.1016/j.jallcom.2015.02.187.
[49] H. Okada, T. Kawanaka, S. Ohmoto, Study on the ZnSe phase diagram by differential thermal analysis, J Cryst Growth 165 (1–2) (1996) 31–36, https://doi.org/10.1016/0022-0248(96)00166-2.
[50] X. Lu, Y. Zhang, J. Ren, et al., Chalcogenide glasses with embedded ZnS nanocrystals: Potential mid-infrared laser host for divalent transition metal ions, J Am Ceram Soc 101 (2) (2018) 666–673, https://doi.org/10.1111/jace.15247.
[51] A.A. Andreev, Z.U. Borisova, E.A. Bichov YGV, Impurity conductivity in chalcogenide glasses doped with iron in equilibrium way by cooling from melt, J Non Cryst Solids 35 (1980) 901–905. & 36.